CH_4 Activation over Perovskite Catalysts: True Density and Reactivity of Active Sites

Felipe Polo-Garzon,*[1] Victor Fung,[2]† Junyan Zhang,[1] Zhenghong Bao,[1]ξ Harry M. Meyer III,[1] Michelle Kidder,[3] Zili Wu*[1][2]

[1]Chemical Sciences Division, Oak Ridge National Laboratory. Oak Ridge, TN 37831 (USA)

[2]Center for Nanophase Materials Sciences, Oak Ridge National Laboratory. Oak Ridge, TN 37831 (USA)

[3]Manufacturing Science Division, Oak Ridge National Laboratory. Oak Ridge, TN 37831 (USA)

ABSTRACT: The high thermal stability of perovskites has drawn attention towards their applications for catalytic CH_4 activation and conversion, typically occurring at high temperatures. The reaction rates of perovskite catalysts for CH_4 combustion, however, trail behind those of noble metal catalysts. Ways to optimize the performance of perovskite catalysts are destined to trial-and-error approaches unless their complex reconstructed surfaces are correlated with fundamental kinetic parameters. Discerning the intrinsic activity of surface catalytic sites, and the density of those sites is crucial to rationally envision complex metal oxides with enhanced catalytic performance. The present work presents a detailed kinetic analysis of catalytic CH_4 combustion over a set of 7 perovskites ($SrTiO_3$, $SrZrO_3$, $SrFeO_3$, $LaFeO_3$, $LaInO_3$, $LaCoO_3$, $LaMnO_3$) with various surface terminations. Steady-state isotopic transient kinetic analysis (SSTIKA) was employed to measure turnover frequency (TOF) and density of surface intermediates (*N*) under operando conditions. Top surface characterization elucidated performance-structure relationships between near-monolayer surface composition and intrinsic reactivity of the catalysts. By using a chemical etching procedure to expose Fe-sites at the top surface of $LaFeO_3$ ($LaFeO_{3,HNO3}$), its TOF was increased 4-fold, compared with the unmodified sample, although *N* on the surface of $LaFeO_{3,HNO3}$ decreased. DFT simulations corroborated that surface Fe-termination and La-Fe termination offer lower energetic barriers for CH_4 activation, when compared with La-termination. In general, surface reconstruction is shown as a tool to tune TOF and *N* to improve reaction rates. This work fills a gap in current kinetic studies of perovskites through a careful assessment and discussion of the density and intrinsic reactivity of active sites for methane combustion over well-characterized reconstructed perovskite surfaces.

KEYWORDS: Perovskites, CH_4 activation, CH_4 combustion, isotopic kinetic analysis, surface reconstruction, surface termination

INTRODUCTION

Recent growth and projected increase in the production of shale gas have motivated renewed interest in the utilization of methane.[1] From an academic standpoint, methane combustion is a simpler reaction network for CH_4 conversion, compared with reforming, coupling, aromatization and others.[2-3] Thus, methane combustion is a suitable reactive system to test reactivity descriptors for catalytic methane activation. From a practical standpoint, elucidating catalysts that completely combust methane at low operating temperatures is crucial for the abatement of pollution, since high temperatures required for flame combustion of methane in air (non-catalytic) lead to production of noxious NO_x gases.[4-5] In addition, unreacted methane is a stronger greenhouse gas than CO_2.[3]

Perovskite catalysts are mixed metal oxides of general formula ABO_3, where A represents a lanthanide, alkaline, or alkaline-earth cation and B represents a transition metal.[6] Perovskites have high thermal stability, required for catalytic CH_4 combustion. However, they are less active than noble metal catalysts. Ample literature has been reported on CH_4 combustion over perovskite catalysts, and it has been reviewed in detail.[2, 7-9] Reports have unveiled catalytic properties that explain differences in the reactivity of a set of perovskites. Catalytic activity for methane oxidation has been associated to the stability of specific metal oxidation states,[10-13] existence of oxygen vacancies,[11, 14-15] oxygen mobility,[12, 15-18] Lewis acid sites,[14] segregation of the A-cation at the surface and the creation of step sites.[19]

Despite the progress made in understanding reactivity trends for sets of perovskites; to-date, the activity of perovskites catalysts for CH_4 activation over an ample range of elemental compositions has not been addressed from a fundamental kinetic standpoint and essential queries remain: What is the intrinsic reactivity (turnover frequency) of the active sites? What is the density of active surface species? And how do they relate to the composition and reconstruction of perovskite catalysts? Answering these questions will enable us to envision superior complex oxide catalysts with high density of highly active catalytic sites. Addressing these fundamental questions demands decoupling the intrinsic reactivity of the active sites (TOF), the density of active sites, and the density of surface intermediates (*N*). The measurement of these kinetic parameters may be skewed if it is not performed under operando conditions, and on the operando reconstructed surface. In the present work, we perform a detailed kinetic study of the intrinsic reactivity of perovskite surfaces, and relate it to the reconstructed catalyst surface. This study reveals fundamental explanations behind macroscopic conversions and reaction

rates observed for a set of 7 perovskites of various elemental compositions and surface reconstructions ($SrTiO_3$, $SrZrO_3$, $SrFeO_3$, $LaFeO_3$, $LaInO_3$, $LaCoO_3$, $LaMnO_3$). These catalysts are chosen as they include two different A-cations (Sr, La) and six different B-cations (Ti, Zr, Fe, In, Co, Mn). Further, this series of perovskites provides a direct comparison of the influence of the A-cation while holding the B-cation constant ($SrFeO_3$ vs. $LaFeO_3$). In addition, this set of perovskites is expected to present a broad range of reaction rates for CH_4 combustion,[2] as will be confirmed later in this manuscript, facilitating the evaluation of reactivity descriptors.

We show that when the perovskite surface is A-terminated (in an 'ABO_3' perovskite), and the B-cation is held constant (Fe), La provides higher TOF than Sr. Upon study of the La-perovskites, we found that exposing Fe at the surface of $LaFeO_3$ led to a 4-fold increase in TOF. This work shows how detailed correlations between operating surface structures and kinetic parameters can be leveraged to design routes for enhancing the intrinsic reactivity.

EXPERIMENTAL DETAILS

Catalysts and materials. $SrTiO_3$ and $SrZrO_3$ were commercially obtained from Sigma Aldrich and Alfa Aesar, respectively. $SrFeO_3$ was synthesized via a sol-gel procedure.[20] $LaFeO_3$,[21] $LaCoO_3$[22-23] and $LaMnO_3$[24] were synthesized using the citrate method. $LaInO_3$ was synthesized by a modified evaporation-induced self-assembly (EISA) approach.[25-26]

For the synthesis of $SrFeO_3$, an ethanol solution of strontium nitrate (with a few drops of water to help dissolve the strontium nitrate) was mixed with an ethanol solution of ferric nitrate with the appropriate mol ratio, and an ethanol solution of oxalic acid at 40 °C for 4 h. The mixture was dried at 150 °C for 24 h. The resulting material was grounded and heated to 500 °C at 6 °C/min, and held for 1 h, then heated to 800 °C at 10 °C/min and held 10 h in a flow of air.

For the synthesis of $LaFeO_3$, $LaCoO_3$ and $LaMnO_3$, a concentrated solution of metal nitrates at proper mol ratio (ca. 0.01 M each) was mixed with an aqueous solution (30-40 mL water) of citric acid (0.02 M) at 40 °C for 30 min. The molar ratio of citric acid to total metal cations was fixed at unity. Water was evaporated from the mixed solution at 80 °C, to obtain a viscous gel. The gel was heated for 12 h at 110 °C (for $LaFeO_3$) or 150 °C (for $LaCoO_3$ and $LaMnO_3$). The resulting glassy material was grounded and heated to 150 °C for 1 h. Next, the material was calcined. For synthesis of $LaFeO_3$, the material was calcined in a flow of air to 800 °C at 5 °C/min and held for 5 h. For $LaCoO_3$, the material was calcined in a flow of air to 500 °C at 6 °C/min and held for 30 min, then up to 700 °C at 10 °C/min and held for 5 h. For $LaMnO_3$, the material was calcined in a flow of air to 500 °C at 6 °C/min and held for 60 min, then up to 750 °C at 10 °C/min and held for 6 h.

$LaInO_3$ was synthesized by a modified evaporation-induced self-assembly (EISA) approach.[25-26] All chemicals were purchased from Sigma-Aldrich and used as received. 1.0825 g $La(NO_3)_3{\cdot}6H_2O$, 1.0221 g $In(NO_3)_3{\cdot}6H_2O$, 4 g Pluronic P-123 (Mn ~ 5800, $EO_{20}PO_{70}EO_{20}$), 6 g Urea were added in alcohol (100g)–water(10g) solution. The mixed homogeneous solution was stirred at 300 RPM and dried at room temperature for 48 h. The resulted precursor was calcined in air by slowly increasing the temperature (1 °C/min) from room temperature to 800 °C and holding at 800 °C for 2 h.

Fe_2O_3 and La_2O_3 were commericially obtained from Sigma Aldrich and Alfa Aesar, respectively.

Gases were purchased from Airgas, except for 2% $^{18}O_2$/He, which was purchased from Sigma-Aldrich.

Chemical etching. $LaFeO_{3,HNO3}$ was synthesized by treating $LaFeO_3$ in a 0.2 M aqueous solution of HNO_3 as implemented in our previous publications.[27-28] Briefly, 0.3 g of $LaFeO_3$ were dissolved in 6 mL of 0.2 M HNO_3 in a vial. The mixture was stirred at room temperature for 1 h at 520 RPM. Next, the sample was washed with deionized water and centrifuged at least three times at 10000 RPM for 5 min. The separated solid was dried in a vacuum oven at 60 °C overnight. Finally, the sample was calcined at 750 °C for 5 h.

$LaFeO_{3,citric}$, $LaMnO_{3,citric}$ and $LaCoO_{3,citric}$ were synthesized by treating $LaFeO_3$, $LaMnO_3$ or $LaCoO_3$ in an aqueous solution of citric acid.[12] 0.3 g of $LaFeO_3$ (or $LaMnO_3$) were dissolved in 6 mL of 1 M citric acid in a vial. The mixture was stirred at room temperature for 1 h at 520 RPM. Next, the sample was washed with deionized water and centrifuged at least three times at 10000 RPM for 5 min. The separated solid was dried in a vacuum oven at 60 °C overnight. Finally, the sample was calcined at 750 °C for 5 h. $LaCoO_{3,citric}$ was prepared by treating 0.45 g of $LaCoO_3$ in 9 mL of 1 M citric acid and following the same procedure.

BET surface area. A Micromeritics Gemini VII Surface Area and Porosity Analyzer was used to measure the surface area of the samples via nitrogen physisorption at -196 °C using the BET method.[29] Before any measurements, the samples were calcined ex situ at 750 °C in air for 5 h.

X-ray diffraction (XRD). A PANalytical Empyrean system was employed for the measurements, using Cu Kα radiation. Incident angles (2θ) were between 5 and 90°. Samples were calcined ex situ at 750 °C for 5 h before performing measurements.

Steady-steady isotopic transient kinetic analysis (SSITKA).

SSITKA experiments were performed in a commercial Altamira Instruments system (AMI-300). 30 mg of each catalyst were diluted in 360 mg of quartz sand. Both catalyst and quartz sand were sieved to 177-250 microns. The catalyst+quartz mixture was loaded to a U-tube reactor and held in place using quartz wool. The catalysts were treated in situ at 750 °C for 5 h under 53 ml/min of 4.2% O_2/He before conducting the reaction at each temperature.

CH_4 combustion was conducted with a "regular feed" of 0.38 % CH_4, 0.38 % Ar, 1.54 % O_2, balance He, and with a "labelled feed" of 0.38 % $^{13}CH_4$, 1.54 % O_2, balance He. The reaction was conducted for 2 h with a "regular feed" (Ar was the tracer accounting for the gas-phase hold-up). After this stabilization period, the inlet of the reactor was switched to "labelled feed". While holding the total flow, temperature, and pressure constant. The transient concentration of reactants and products was monitored using a mass spectrometer (MS) (Pfeiffer Vacuum). The concentration of product in the reactor effluent was quantified using a gas chromatograph (GC) (Buck Scientific). The pressure in the reactor varied with temperature and total feed flow between 1.5 and 2.2 atm. During the isotopic switch, the pressure variation inside the reactor was minimized using back pressure regulators. Conversion was maintained between 7 and 32 % to attain a compromise between differential conditions and good resolution of the MS signals during the SSITKA switch. Reaction rate was found to be dependent on the total flow rate of the feed, therefore, rate per surface area, conversions and *N* are reported for a total inlet flow rate of 91 mL/min.

TOF and *N* were calculated exclusively for CO_2 as it is the main product (CO was the secondary product). The surface

residence time (τ) of species involved in CO_2 production was measured using the normalized transient of CO_2 (m/z=44) during the isotopic switch. To obtain the real surface residence time (τ_0), τ was measured at different total flows (65-117 mL/min), and the value was extrapolated to infinite flow. Assuming pseudo-first-order irreversible reaction with a single-intermediate pool, TOF is calculated as $1/\tau_0$. The density of surface intermediates, N, is calculated as N = [rate CO_2 production] × τ_0.[30-31] The observed kinetic isotopic effect of $^{13}CH_4$ was not significant. The error of TOF measured at a certain temperature is obtained from the error of the intercept in linear regression τ vs. 1/Flow rate. The error of TOF calculated through interpolation or extrapolation at different temperatures is obtained from reference [32].

Low-energy ion scattering (LEIS). LEIS measurements were performed at Lehigh University in an ION-TOF Qtac100 spectrometer. Before LEIS analysis, the samples were calcined ex situ at 750 °C for 5 h, and then pressed into a crucible at a pressure of 2000 psi. The samples were then loaded into the LEIS chamber, where they were heated in 10 mbar of O_2 at 500 °C for 1 h. Samples were sputtered to a depth of approximately 2 nm using an Ar beam and spectra were acquired at each 0.2 nm increment. Charge neutralization was invoked during spectra acquisition and sputtering using a beam of low energy electrons. Spectra were collected using 5 keV Ne^+ at 2 x 10^{14} ions/cm^2 per profile cycle. Sputter of the samples, to obtain the depth profile, was done using 0.5 keV Ar^+ at 8 x 10^{14} ions/cm^2 per profile cycle. Quantification of La and Sr in the samples was done using the relative sensitivity factor (RSF) of neighboring elements (Hf and Zr, respectively). LEIS compositions are reported in atomic percentage and oxygen-free basis. An ion beam of 3 keV He^+ 2 x 10^{14} ions/cm^2 was used to scan samples for nitrogen (possibly remaining after chemical etching).

Inductively coupled plasma (ICP) measurements. ICP measurements were performed by Galbraith Laboratories, Inc.

X-ray photoelectron spectroscopy (XPS). Before XPS analysis, the samples were calcined ex situ at 750 °C for 5 h. XPS was performed using a Thermo Scientific (Waltham, MA, USA) Model K-Alpha XPS instrument. The instrument utilizes monochromated, micro-focused, Al K_α X-rays (1486.6 eV) with a variable spot size (i.e., 30-400 µm). Analysis of the sample was performed with the 400 µm X-ray spot size for maximum signal and to obtain an average surface composition over the largest possible area. The instrument has a hemispherical electron energy analyzer equipped with a 128-channel detector system. Base pressure in the analysis chamber is typically 2 x 10^{-9} mbar or lower.

Adsorption microcalorimetry. Adsorption microcalorimetry of CO_2 was performed using a Micromeritics 3Flex Characterization Analyzer coupled with a Setaram Sensys Evo DSC microcalorimeter. Each sample was evacuated at 30 °C for approximately 1 h, next, the chamber was filled with 500 mmHg of O_2 and the temperature was raised to 750 °C at 10 °C/min. Once at 750 °C, the sample was maintained under O_2 for ~ 2.5 h, evacuated for 30 min, exposed to 500 mmHg of O_2 again for approximately ~ 2 h, and evacuated for ~3 h. The sample temperature was then lowered to 30 °C while evacuating. Next, CO_2 was dosed to perform the measurements. After the final target pressure was reached, the sample was evacuated for 1 h at the same temperature (30 °C) and CO_2 was dosed again. The concentration of the adsorption sites was determined by the amount of irreversibly adsorbed CO_2.

Temperature-programmed reduction (TPR). TPR experiments were performed in an AMI-300 unit. 20 mg of each catalyst were loaded in a U-tube and held in place by quartz wool. The samples were pretreated in situ at 750 °C for 5 h under 53 ml/min of 4.2 % O_2/He. The gas flowing through the sample was switched to He and the temperature was lowered to 50 °C. Next, 40 mL/min of 4% H_2/Ar were flowed through the sample and the temperature was ramped from 50 °C to 900 °C at a rate of 10 °C/min. The consumption of H_2 was monitored via MS.

Temperature-programmed $^{18}O_2$-exchange (TPOX). TPOX experiments were performed in a commercial Altamira Instruments system (AMI-200). 30 mg of each sample diluted in quartz sand (1:12 dilution ratio) were loaded into a U-tube reactor. The catalyst sample was pretreated in situ for 5 h at 750 °C under 50 mL/min of 4.5% O_2/He. The sample was cooled down to ~50 °C, the gas atmosphere was switched to 50 mL/min of 1.8 % $^{18}O_2$/He, and the temperature was ramped to ~750 °C at 11 °C/min. The exchange of $^{18}O_2$ and $^{16}O_2$ was monitored via MS.

Diffuse reflectance infrared Fourier transform spectroscopy (DRIFTS). Before DRIFTS measurements, the perovskite samples were calcined ex situ at 750 °C for 5 h, and the reference samples (La_2O_3, Fe_2O_3) were calcined ex situ at 300 °C for 2 h. DRIFTS was performed with a Nicolet Nexus 670 FTIR spectrometer. Each sample was loaded into the DRIFTS cell (Pike technologies) and pretreated in situ at 300 °C under 30 mL/min of Ar flow for 45 min. Next, the temperature was lowered to 25 °C and a background spectrum was collected. The sample was then exposed to methanol at 25 °C for 10 min (30 mL/min of Ar flowing through a bubbler containing methanol at room temperature). Next, the sample was flushed with 30 mL/min Ar for 18 min to desorb methanol. Spectra were collected during the adsorption/desorption process.

Density functional theory (DFT) calculations. Calculations were performed using the Vienna Ab Initio Simulation Package (VASP).[33-34] The projector-augmented wave method was used to describe the electron-core interaction.[33, 35] A kinetic energy cutoff of 450 eV was used. The Perdew-Burke-Ernzerhof (PBE)[36] functional form of generalized-gradient approximation (GGA) was used for electron exchange and correlation energies. Dispersion corrections were added using the method by Grimme.[37] A 2×2×1 sampling of Brillouin zone using a Monkhorst-Pack scheme was used for the k-points.[38] A vacuum layer of 15 Å was used for the surface slabs. Transition states (TS) were found with the nudged elastic band (NEB)[39] with a force convergence criterion of 0.05 eV/Å.

TOF, was 58 kJ/mol for $SrTiO_3$, whereas it laid between 27 and 43 kJ/mol for the other catalysts. This suggests that CH_4 combustion over $SrTiO_3$ may proceed via a different reaction mechanism. In addition, $SrTiO_3$ was the catalyst with the lowest intrinsic activity (TOF, **Fig. 2, Fig. S10**). A correlation between TOF, *N* and rates was not observed amongst the seven perovskites, showing the importance of fundamentally

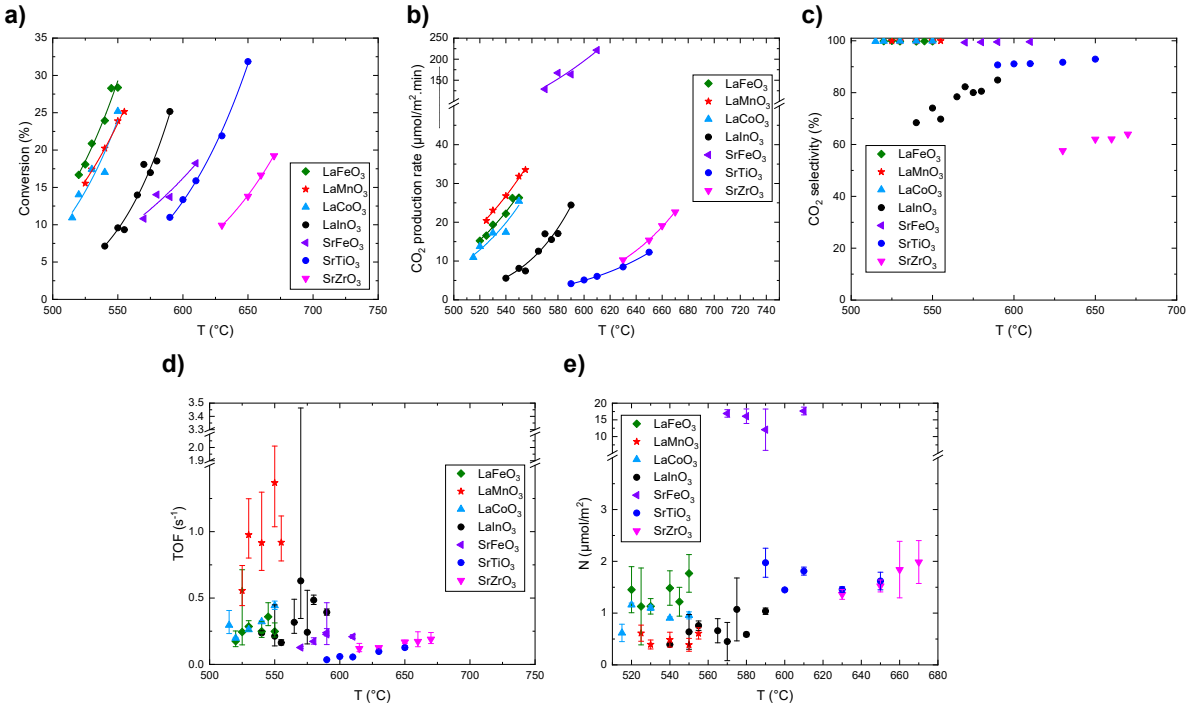

Fig. 1 CH_4 combustion over perovskites. **a)** conversion, **b)** rate, **c)** CO_2 selectivity, **d)** TOF, **e)** *N*.

RESULTS AND DISCUSSION

Seven perovskite catalysts of various elemental compositions ($SrTiO_3$, $SrZrO_3$, $SrFeO_3$, $LaFeO_3$, $LaInO_3$, $LaCoO_3$, $LaMnO_3$) and crystal structures (**Fig. S1**) were tested for CH_4 combustion. According to XRD characterization, the chemical formula of some samples deviates slightly from "ABO_3" (**Fig. S1**). However, in the manuscript we refer to all samples with the ideal ABO_3 composition for simplificity. BET surface areas were between 1 and 19 m^2/g (**Table S1**). Samples were pretreated in O_2 at 750 °C for 5 h before kinetic measurements and characterization, as this pre-treatment time and temperature are expected to achieve stably reconstructed catalysts,[40] thus preventing reconstruction during experimentation. **Fig. 1a,b,c** show the obtained conversion, rate per surface area and selectivity to CO_2. Ranking catalysts from "most active" to "least active" depends on how "activity" is defined: conversion, rate per surface area, rate per mass, etc. Here, we will deep-dive into the most fundamental definition of activity: the activity per active site (TOF). SSITKA experiments were performed to find TOF and *N* at various temperatures (**Fig. 1d,e**, **Fig. S2-S8**). Since the catalysts under study provide low conversions at different temperature regimes, we used simple extrapolation using the Arrhenius equation to compare TOF, *N* and rates at 550 °C and 625 °C (**Fig. 2, Fig. S9-S10**). Activation energies estimated from the regression log(TOF) vs. 1/T differed from those estimated from the regression log(Rate) vs. 1/T (**Fig. S9**). This difference could be rooted in the change of surface intermediate density with temperature (**Fig. 1e**). The activation energy, estimated from differentiating intrinsic activity and density of active sites/intermediates.

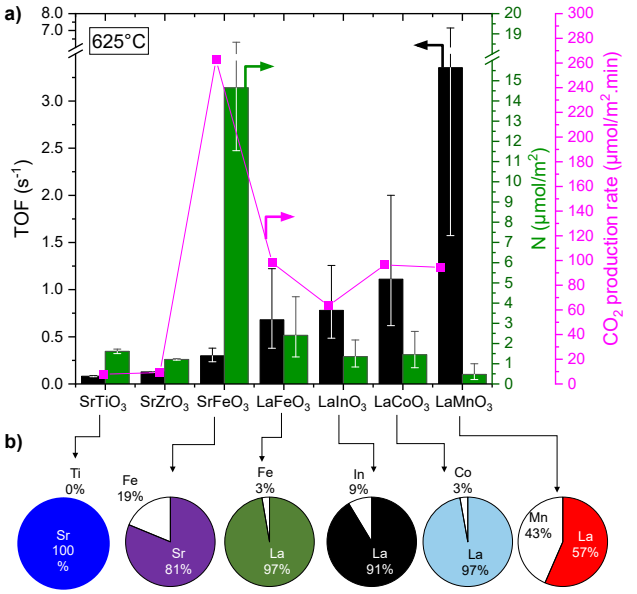

Fig. 2 a) TOF, *N* (density of surface intermediates) and rate for CH_4 combustion over perovskites at 625 °C. **b)** Top surface composition of perovskites measured via LEIS *(Some La was present in $SrTiO_3$ due to sample contamination during LEIS. See **Fig. S11** and associated text presenting ICP and XPS results).*

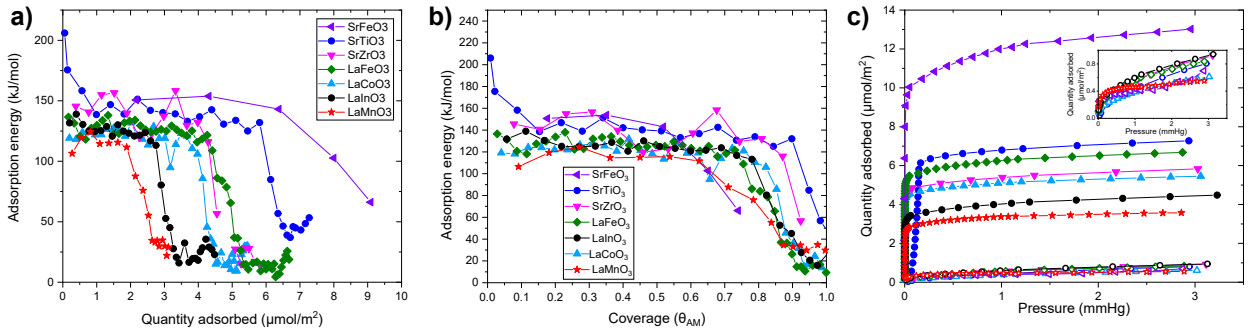

Fig. 3 Adsorption microcalorimetry results. **a)** Adsorption energy as a function of moles adsorbed per unit area. **b)** Adsorption energy as a function of partial coverage of the surface (θ_{AM}).**c)** Moles adsorbed per unit area as a function of pressure: on clean surface (solid symbols) and upon readsorption (hollow symbols, see inset for zoomed-in image). *Replicas are not shown.*

Our previous work on CH_4 activation over reconstructed $SrTiO_3$ catalysts suggested that basic SrO-sites are the active sites for CH_4 activation.[19, 41] Titration of basic sites can be done using the main product of CH_4 combustion, CO_2, which is presumed to provide a reasonable estimate of available surface sites. Adsorption microcalorimetry was used to quantify the density of adsorption sites for CO_2 and the strength of adsorption (**Fig. 3**, **Table 1**, **Fig. S12**)

Table 1 Adsorption microcalorimetry results

Catalyst	CO_2 adsorption Energy (kJ/mol)	CO_2 adsorption sites (μmol/m²)
$SrTiO_3$	131 ± 13†	6.7 ± 0.2†
$SrZrO_3$	140	4.9
$SrFeO_3$	139 ± 10†	14.3 ± 2.1†
$LaFeO_3$	128	5.8
$LaInO_3$	136 ± 9†	3.6 ± 0.0†
$LaCoO_3$	123	4.8
$LaMnO_3$	116	3.0

† Average of two replicas

Table 1 presents an average of the adsorption energy for surface coverage during adsorption microcalorimetry (θ_{AM}) between 5% and 60%, and it is intended to provide an estimate of the adsorption strength for the majority of adsorption sites (see **Fig. 3a,b**, **Fig. S12**). Based on the uncertainty obtained when replicas of the measurements were performed ($SrTiO_3$, $SrFeO_3$ and $LaInO_3$ in**Table 1**), we conclude that the adsorption strength of CO_2 on the catalysts is not significantly different. Therefore, the strength of basic sites is not concluded as a descriptor for TOF. The density of adsorption sites for chemisorption of CO_2 can be measured by repeating the adsorption microcalorimetry experiment, after vacuuming the chamber at room temperature to desorb physisorbed species (**Fig. 3c**). The density of adsorption sites for CO_2 correlates with the density of surface intermediates (N) (**Fig. 4a**). The coverage of surface intermediates (θ^N) on available adsorption sites can be estimated as: $\theta^N = N/[CO_2 \text{ adsorption sites}]$ (**Fig. 4b**). N, and thus θ^N, increase with temperature for all catalysts except for $SrTiO_3$ and $SrFeO_3$. The increase of N with temperature has been observed before, and it has been attributed to the fact that at higher temperatures more sites become active sites.[42-43] Most importantly, the adsorption sites on $SrFeO_3$ are ~100 % occupied by surface intermediates. This explains the superior rate per surface area of $SrFeO_3$ (**Fig. 1b**). Namely, $SrFeO_3$ has the highest density of available surface active sites (**Table 1**), and nearly all surface sites host active surface intermediates (**Fig. 4b**). Active surface intermediates on other perovskites occupy less than 40 % of available sites. Although $LaMnO_3$ has a very low occupancy of surface sites (**Fig. 4b**), it presented the second highest rate per surface area (**Fig. 1b**) due to the superior TOF (**Fig. 2, Fig. S10**).

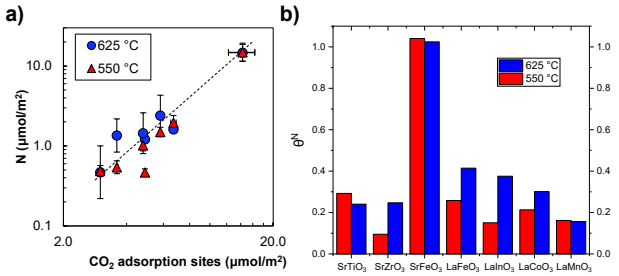

Fig. 4 a) N versus CO_2 adsorption sites, **b)** surface coverage by active intermediates (θ^N).

Now, we take a closer look at TOFs presented in **Fig. 2a**. In the x-axis of **Fig. 2a**, catalysts are ordered from low TOF to high TOF from left to right. An initial comparison can be drawn between $SrFeO_3$ and $LaFeO_3$, which share the same B-cation and are predominantly A-terminated at the surface as characterized via LEIS with near-monolayer sensitivity (81 % Sr for $SrFeO_3$ and 97 % La for $LaFeO_3$, **Fig. 2b, Fig. S11**). TOF of $LaFeO_3$ is more than twice that of $SrFeO_3$ (0.68 versus 0.30 s^{-1}); however, the density of surface species of $SrFeO_3$ is 6-fold that of $LaFeO_3$ (14.6 versus 2.4 μmol/m²). When the surface termination of $LaFeO_3$ is adjusted to 86 % (sample $LaFeO_{3,HNO3}$ later discussed in the text) to compare with the 81 % Sr-terminated $SrFeO_3$, TOF of the lanthanum sample is even higher.

In general, TOF of the La-catalysts ($LaFeO_3$, $LaInO_3$, $LaCoO_3$, $LaMnO_3$) is superior to the TOF of the Sr-catalysts ($SrTiO_3$, $SrZrO_3$, $SrFeO_3$). $LaMnO_3$ presented the highest TOF, nearly 3-fold that of $LaCoO_3$ (second highest TOF) at 625 °C, and the lowest N (**Fig. 2a**). Similar trends were observed at 550 °C (**Fig. S10).** For the Sr-containing samples, Sr and Zr signals were undistinguishable using LEIS. $SrFeO_3$ had more B-cations at the surface (19%) than $SrTiO_3$ (0%), but both samples were predominantly A-terminated. The surface termination of the

catalyst with the highest TOF, $LaMnO_3$, was 57 % La and 43 % Mn, which was the closest to the stoichiometric bulk concentration (50 %/50 %). We hypothesize that the highest TOF is attained on B or synergistic A-B sites present on the surface of $LaMnO_3$.

Before testing our hypothesis, we evaluated other reactivity descriptors reported in the literature: reducibility of the catalyst and oxygen mobility. TPR experiments were conducted to assess the reducibility of the surface (reduction temperature) and the extent of reduction (H_2 moles consumed). No correlation to TOF or *N* was found (**Fig. S13**). For instance, $LaFeO_3$ presented negligible reduction during TPR, yet its TOF and *N* were not the lowest **(Fig. 2a**, **Fig. S10**). Next, the oxygen mobility of select catalysts with low and high TOF ($SrTiO_3$, $SrZrO_3$, $LaCoO_3$, $LaMnO_3$) was evaluated via $^{18}O_2$-exchange experiments (TPOX, **Fig. S14**). The ease of exchange, related to the onset temperature, and the extent of exchange (^{18}O moles exchanged per ^{16}O mol in the lattice) did not correlate with TOF or *N*. For instance, $LaMnO_3$ and $SrTiO_3$ have the highest and the lowest TOF respectively (**Fig. 2a**, **Fig. S10**); however, the temperature for the onset of oxygen mobility is much higher for $LaMnO_3$ than for $SrTiO_3$. *N* is very similar for $SrZrO_3$ and $LaCoO_3$ (**Fig. 2a**, **Fig. S10**); however, the amount of oxygen exchanged up to ~755 °C for $LaCoO_3$ is 5 times that of $SrZrO_3$ (**Fig. S14**). *N* for $SrZrO_3$ is equal or higher than for $LaMnO_3$; however, $SrZrO_3$ presents the lowest oxygen mobility in terms of onset temperature and moles exchanged (**Fig. S14**). The fact that reducibility and oxygen mobility do not correlate with TOF and *N*, does not mean these catalyst properties are irrelevant for the catalytic cycle. Instead, it means that for the set of perovskites studied, within the reaction conditions evaluated, the reaction rate is described by other catalyst properties, which would ultimately be a reactivity descriptor. Other work has also suggested no simple correlation between redox properties of the catalyst and the rates for CH_4 oxidation[44]

Indeed, $LaFeO_{3,HNO3}$ showed higher TOF than $LaFeO_3$ (4-fold) but $LaFeO_{3,HNO3}$ also showed a reduction in *N*. TOF and *N* reported here are "global" values accounting for the contribution from A and B sites. The fact that TOF grows with the exposure of B sites (**Fig. 5**) suggests an increased contribution from the more active B-sites to "global" TOF. However, the density of surface intermediates (*N*) decreases as more B-sites are exposed. This evidences a trade-off between TOF and *N*. Modulating these two kinetic parameters allows to maximize reaction rates. Breaking this trade-off to attain high TOF and high *N* demands further studies that lie beyond the scope of this work.

For the comparison presented in **Fig. 5a**, we re-measured TOF, *N* and rate for the base $LaFeO_3$ catalyst, as our experimental setup underwent changes in-between collection of data presented in **Fig. 1** and **Fig. 5**. Small variations did not affect the conclusions presented (**Fig. S16**). To manipulate the extent of etching of the surface, $LaFeO_3$ was treated with citric acid (sample $LaFeO_{3,citric}$). LEIS analysis with an He^+ ion beam did not detect any residual nitrogen on the surface after acid treatment (HNO_3 or citric acid). Na and S contamination was detected both in the base and the acid-treated samples. Interestingly, treatment with citric acid increased the concentration of La at the very top surface (100 % La) but etched La away in the sublayers (**Fig. 5b,c**). $LaFeO_{3,\ citric}$ showed the lowest TOF and the highest *N*, when comparing $LaFeO_3$ samples with different surface compositions (**Fig. 5a**), which further supports that the composition of the *top-monolayer* is a descriptor for the intrinsic reactivity of the surface. La top-surface composition of $LaFeO_3$ samples (**Fig. 5**), measured via LEIS, varied in a narrow range (86-100%). Therefore, we used DRIFTS of methanol (probe molecule) adsorption to corroborate the trends obtained via LEIS. Detailed DRIFTS results can be found in **Fig. S17** and associated text. DRIFTS results support LEIS characterization.

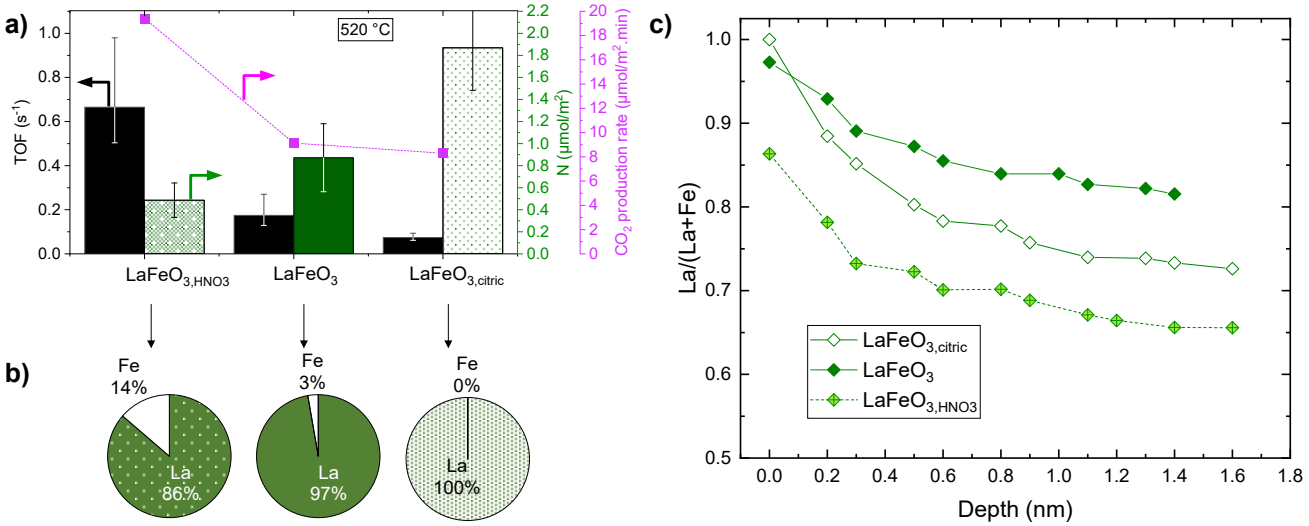

Fig. 5 a) TOF, *N* and rate for CH_4 combustion over $LaFeO_{3,HNO3}$, $LaFeO_3$ and $LaFeO_{3,citric}$ at 520 °C. **b)** Top surface composition measured via LEIS. **c)** Depth profile measured via LEIS.

Now that reducibility and oxygen mobility of the catalysts have been ruled out as descriptors for TOF and *N*, we proceed to test our hypothesis that B sites or synergistic A-B sites have enhanced TOF. The surface of $LaFeO_3$ (97% La) was chemically etched with HNO_3 to expose Fe cations at the surface, as confirmed via LEIS (**Fig. 5**), while conserving the crystal structure (**Fig. S15**). This sample is named $LaFeO_{3,HNO3}$.

To discern whether a Fe- or La/Fe-terminated sites provide the highest intrinsic activity, we performed DFT simulations for C-H bond dissociation in methane over three different crystallographic terminations (**Table 2**, **Fig. 6**). We assume C-H dissociation is the rate-determining step, as we found no correlation between TOF and oxygen mobility/reducibility (**Fig. 2a, Fig. S13-S14**). (100) and (210)

facets offer La or Fe terminations, whereas the (110) facet offers a combined La-Fe termination. The lowest activation energies occur on Fe-terminated (100) and (210) facets (0.73 and 0.75 eV, respectively), suggesting that the Fe-termination is more active for CH_4 activation. However, the Fe-La-O termination had a moderate activation energy of 1.29 eV, lower than the activation barrier on La-termination. Therefore, we conclude that Fe-sites are responsible for enhanced TOF, with a possible minor contribution from Fe-La sites.

Table 2 C-H activation barriers and reaction energies.

Facet	Termination	Pathway	E_{act}	ΔH
100	La	Homolytic	3.22	3.22
	Fe	Homolytic	2.12	2.06
	La	Heterolytic	1.61	1.61
	Fe	**Heterolytic**	**0.73**	**0.43**
110	Fe-La-O	Homolytic	2.72	2.72
	O	Homolytic	1.55	1.55
	Fe-La-O	**Heterolytic**	**1.29**	**0.45**
210	La step	Homolytic	2.12	1.92
	Fe step	**Heterolytic**	**0.75**	**-0.33**

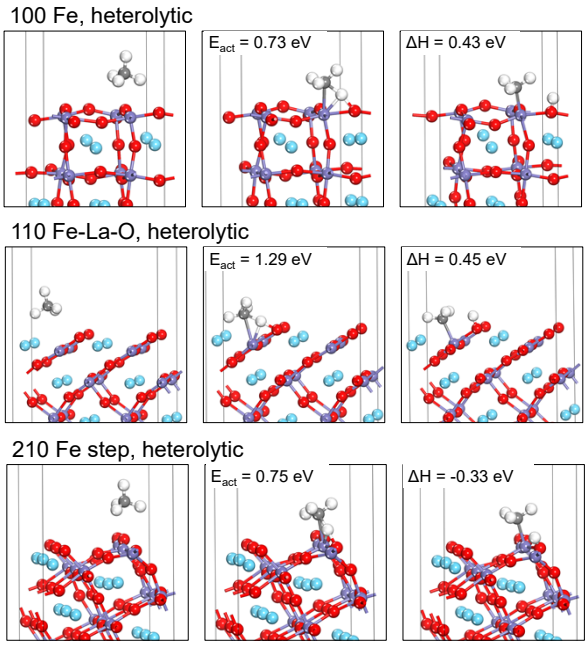

Fig. 6 Initial, transition state and final configurations (left-to-right) for CH_4 activation. Structures with lowest activation energies (see Table 2). Color code: C-gray, H-white, O-red, Fe-purple, La-blue.

Treating $LaFeO_3$ and $LaMnO_3$ in citric acid resulted in increased concentration of La at the top surface; however, treatment of $LaCoO_3$ in citric acid resulted in depletion of La at the top surface (**Fig. S18**). Tuning the surface composition of $LaMnO_3$ and $LaCoO_3$ also affected their TOF, with a minor influence on *N* (**Fig. S21a,b**). It is evident that fundamentally understanding the interaction of etching agents with different perovskite surfaces to predict reconstruction behaviors grants a thorough study on its own. Further, although we observed proportionality between TOF and the concentration of the B-cation at the top surface of $LaFeO_3$ (**Fig. 5**), this was not the case for $LaMnO_3$ (**Fig. S21**). Compilation of TOF versus surface termination of 8 La-perovskites studied here suggests a nonmonotic dependence of TOF with surface termination (**Fig. S21**) but further studies to understand this dependence are necessary.

CONCLUSIONS

The present work presents a detailed kinetic analysis of CH_4 combustion over a set of perovskite catalysts with various crystal structures, elemental compositions, and surface reconstructions. Turnover frequencies (TOF) and density of surface intermediates (*N*) were measured under operando conditions via SSITKA. Comparison of $SrFeO_3$ and $LaFeO_3$ with predominantly A-termination shows that La promotes higher TOF than Sr. Adsorption microcalorimetry measurements allowed to correlate *N* with the adsorption sites for CO_2; however, the strength of adsorption (related to the strength of surface basicity) was not correlated with TOF. Increasing the concentration of Fe at the surface (86 % La, 14 % Fe) of $LaFeO_3$ increased TOF 4-fold, compared with the base La-terminated (97 % La, 3 % Fe) $LaFeO_3$ catalyst. Increase in TOF was accompanied by a reduction of *N*, showing that for the same perovskite structure (i.e., $LaFeO_3$), tuning the top-monolayer surface composition affects both the intrinsic reactivity of the surface and the density of surface intermediates. In conclusion, overall reaction rates are a compromise between TOF and *N*, which can be adjusted via surface reconstruction. Revolutionary ideas to break this compromise are needed to push the boundaries of methane catalysis over perovskites.

AUTHOR INFORMATION

Corresponding Authors
*F.P. pologarzonf@ornl.gov
*Z.W. wuz1@ornl.gov

Present Addresses
†Victor Fung: School of Computational Science and Engineering, Georgia Institute of Technology. Atlanta, GA 30332 (USA).
ξZhenghong Bao: Department of Orthopaedics, West Virginia University. Morgantown, WV 26506 (USA).

Author Contributions
All authors have given approval to the final version of the manuscript.

ASSOCIATED CONTENT

Supporting Information.
XRD, BET surface areas, SSITKA results, adsorption microcalorimetry, LEIS, DRIFTS, TPR, TPOX.
This material is available free of charge via the Internet at http://pubs.acs.org.

ACKNOWLEDGEMENT

This research was sponsored by the U.S. Department of Energy, Office of Science, Office of Basic Energy Sciences, Chemical Sciences, Geosciences, and Biosciences Division, Catalysis

Science program. Some of the work including kinetic measurements, temperature-programmed catalyst characterization, and DFT simulations was conducted as part of a user project at the Center for Nanophase Materials Sciences, which is a US Department of Energy, Office of Science User Facility at Oak Ridge National Laboratory. We thank Dr. Ryan Thorpe (Lehigh University) for performing LEIS analysis.

Notes

The authors declare no competing financial interest.

REFERENCES

1. Administration, U. S. E. I.; Analysis, O. o. E.; Energy, U. S. D. o.; Washington, D., Annual Energy Outlook 2018

with projections to 2050. **2018**.

2. Royer, S.; Duprez, D.; Can, F.; Courtois, X.; Batiot-Dupeyrat, C.; Laassiri, S.; Alamdari, H., Perovskites as Substitutes of Noble Metals for Heterogeneous Catalysis: Dream or Reality. *Chemical Reviews* **2014,** *114* (20), 10292-10368.

3. Taifan, W.; Baltrusaitis, J., CH4 conversion to value added products: Potential, limitations and extensions of a single step heterogeneous catalysis. *Applied Catalysis B: Environmental* **2016,** *198*, 525-547.

4. Chen, J.; Arandiyan, H.; Gao, X.; Li, J., Recent Advances in Catalysts for Methane Combustion. *Catal. Surv. Asia* **2015,** *19* (3), 140-171.

5. Choudhary, T. V.; Banerjee, S.; Choudhary, V. R., Catalysts for combustion of methane and lower alkanes. *Appl. Catal. A: Gen.* **2002,** *234* (1), 1-23.

6. Zhu, H.; Zhang, P.; Dai, S., Recent Advances of Lanthanum-Based Perovskite Oxides for Catalysis. *ACS Catalysis* **2015,** *5* (11), 6370-6385.

7. Bashan, V.; Ust, Y., Perovskite catalysts for methane combustion: applications, design, effects for reactivity and partial oxidation. *International Journal of Energy Research* **2019,** *43* (14), 7755-7789.

8. Ladavos, A.; Pomonis, P., Methane Combustion on Perovskites. In *Perovskites and Related Mixed Oxides*, Wiley-VCH Verlag GmbH & Co. KGaA: 2016.

9. Yang, J.; Guo, Y., Nanostructured perovskite oxides as promising substitutes of noble metals catalysts for catalytic combustion of methane. *Chinese Chemical Letters* **2018,** *29* (2), 252-260.

10. Ponce, S.; Peña, M. A.; Fierro, J. L. G., Surface properties and catalytic performance in methane combustion of Sr-substituted lanthanum manganites. *Applied Catalysis B: Environmental* **2000,** *24* (3), 193-205.

11. Pecchi, G.; Jiliberto, M. G.; Buljan, A.; Delgado, E. J., Relation between defects and catalytic activity of calcium doped LaFeO3 perovskite. *Solid State Ionics* **2011,** *187* (1), 27-32.

12. Ding, Y.; Wang, S.; Zhang, L.; Chen, Z.; Wang, M.; Wang, S., A facile method to promote LaMnO3 perovskite catalyst for combustion of methane. *Catalysis Communications* **2017,** *97*, 88-92.

13. Najjar, H.; Batis, H.; Lamonier, J.-F.; Mentré, O.; Giraudon, J.-M., Effect of praseodymium and europium doping in La1−xLnxMnO3+δ (Ln: Pr or Eu, 0≤x≤1) perosvkite catalysts for total methane oxidation. *Applied Catalysis A: General* **2014,** *469*, 98-107.

14. Yang, J.; Hu, S.; Shi, L.; Hoang, S.; Yang, W.; Fang, Y.; Liang, Z.; Pan, C.; Zhu, Y.; Li, L.; Wu, J.; Hu, J.; Guo, Y., Oxygen Vacancies and Lewis Acid Sites Synergistically Promoted Catalytic Methane Combustion over Perovskite Oxides. *Environmental Science & Technology* **2021,** *55* (13), 9243-9254.

15. Li, C.; Wang, W.; Zhao, N.; Liu, Y.; He, B.; Hu, F.; Chen, C., Structure properties and catalytic performance in methane combustion of double perovskites Sr2Mg1−xMnxMoO6−δ. *Applied Catalysis B: Environmental* **2011,** *102* (1), 78-84.

16. Kirchnerova, J.; Alifanti, M.; Delmon, B., Evidence of phase cooperation in the LaCoO3–CeO2–Co3O4 catalytic system in relation to activity in methane combustion. *Applied Catalysis A: General* **2002,** *231* (1), 65-80.

17. Royer, S.; Alamdari, H.; Duprez, D.; Kaliaguine, S., Oxygen storage capacity of La1−xA′xBO3 perovskites (with A′=Sr, Ce; B=Co, Mn)—relation with catalytic activity in the CH4 oxidation reaction. *Applied Catalysis B: Environmental* **2005,** *58* (3), 273-288.
18. Chang, H.; Bjørgum, E.; Mihai, O.; Yang, J.; Lein, H. L.; Grande, T.; Raaen, S.; Zhu, Y.-A.; Holmen, A.; Chen, D., Effects of Oxygen Mobility in La–Fe-Based Perovskites on the Catalytic Activity and Selectivity of Methane Oxidation. *ACS Catalysis* **2020,** *10* (6), 3707-3719.
19. Polo-Garzon, F.; Fung, V.; Liu, X.; Hood, Z. D.; Bickel, E. E.; Bai, L.; Tian, H.; Foo, G. S.; Chi, M.; Jiang, D.-e.; Wu, Z., Understanding the Impact of Surface Reconstruction of Perovskite Catalysts on CH4 Activation and Combustion. *ACS Catalysis* **2018,** *8* (11), 10306-10315.
20. Jaiswal, S. K.; Kashyap, V. K.; Kumar, J., On the sol–gel synthesis and characterization of strontium ferrite ceramic material. *Materials Research Bulletin* **2012,** *47* (3), 692-699.
21. Ciambelli, P.; Cimino, S.; De Rossi, S.; Lisi, L.; Minelli, G.; Porta, P.; Russo, G., AFeO3 (A=La, Nd, Sm) and LaFe1−xMgxO3 perovskites as methane combustion and CO oxidation catalysts: structural, redox and catalytic properties. *Applied Catalysis B: Environmental* **2001,** *29* (4), 239-250.
22. Sartipi, S.; Khodadadi, A. A.; Mortazavi, Y., Pd-doped LaCoO3 regenerative catalyst for automotive emissions control. *Applied Catalysis B: Environmental* **2008,** *83* (3), 214-220.
23. Guo, X.; Meng, M.; Dai, F.; Li, Q.; Zhang, Z.; Jiang, Z.; Zhang, S.; Huang, Y., NOx-assisted soot combustion over dually substituted perovskite catalysts La1−xKxCo1−yPdyO3−δ. *Applied Catalysis B: Environmental* **2013,** *142-143*, 278-289.
24. Taguchi, H.; Matsu-ura, S.-i.; Nagao, M.; Choso, T.; Tabata, K., Synthesis of LaMnO3+δby Firing Gels Using Citric Acid. *Journal of Solid State Chemistry* **1997,** *129* (1), 60-65.
25. Zhao, F.; Liu, Q.; Wang, S.; Chen, F., Infiltrated multiscale porous cathode for proton-conducting solid oxide fuel cells. *Journal of Power Sources* **2011,** *196* (20), 8544-8548.
26. Huang, X.; Zhao, G.; Wang, G.; Irvine, J. T. S., Synthesis and applications of nanoporous perovskite metal oxides. *Chem Sci* **2018,** *9* (15), 3623-3637.
27. Polo-Garzon, F.; Yang, S. Z.; Fung, V.; Foo, G. S.; Bickel, E. E.; Chisholm, M. F.; Jiang, D. e.; Wu, Z., Controlling Reaction Selectivity through the Surface Termination of Perovskite Catalysts. *Angew. Chem.* **2017,** *129* (33), 9952-9956.
28. Foo, G. S.; Hood, Z. D.; Wu, Z., Shape Effect Undermined by Surface Reconstruction: Ethanol Dehydrogenation over Shape-Controlled $SrTiO_3$ Nanocrystals. *ACS Catal.* **2018,** *8* (1), 555-565.
29. Brunauer, S.; Emmett, P. H.; Teller, E., Adsorption of Gases in Multimolecular Layers. *J. Am. Chem. Soc.* **1938,** *60* (2), 309-319.
30. Shannon, S. L.; Goodwin, J. G., Characterization of Catalytic Surfaces by Isotopic-Transient Kinetics during Steady-State Reaction. *Chemical Reviews* **1995,** *95* (3), 677-695.
31. Ledesma, C.; Yang, J.; Chen, D.; Holmen, A., Recent Approaches in Mechanistic and Kinetic Studies of Catalytic Reactions Using SSITKA Technique. *ACS Catalysis* **2014,** *4* (12), 4527-4547.
32. Kirchner, J. seismo.berkeley.edu/~kirchner/eps_120/Toolkits/Toolkit_10.pdf.
33. Kresse, G.; Furthmuller, J., Efficiency of Ab-Initio Total Energy Calculations for Metals and Semiconductors Using a Plane-Wave Basis Set. *Comput. Mater. Sci.* **1996,** *6* (1), 15-50.
34. Kresse, G.; Furthmuller, J., Efficient Iterative Schemes for Ab Initio Total-Energy Calculations Using a Plane-Wave Basis Set. *Phys. Rev. B* **1996,** *54* (16), 11169-11186.
35. Blöchl, P. E., Projector Augmented-Wave Method. *Phys. Rev. B* **1994,** *50* (24), 17953-17979.
36. Perdew, J. P.; Burke, K.; Ernzerhof, M., Generalized Gradient Approximation Made Simple. *Phys. Rev. Lett.* **1996,** *77* (18), 3865-3868.
37. Grimme, S.; Antony, J.; Ehrlich, S.; Krieg, H., A Consistent and Accurate ab Initio Parametrization of Density Functional Dispersion Correction (DFT-D) for the 94 Elements H-Pu. *J. Chem. Phys.* **2010,** *132* (15), 154104.

38. Monkhorst, H. J.; Pack, J. D., Special Points for Brillouin-Zone Integrations. *Phys. Rev. B* **1976,** *13* (12), 5188-5192.
39. Henkelman, G.; Uberuaga, B. P.; Jónsson, H., A Climbing Image Nudged Elastic Band Method for Finding Saddle Points And Minimum Energy Paths. *J. Chem. Phys.* **2000,** *113* (22), 9901-9904.
40. Polo-Garzon, F.; Yang, S.-Z.; Fung, V.; Foo, G. S.; Bickel, E. E.; Chisholm, M. F.; Jiang, D.-e.; Wu, Z., Controlling Reaction Selectivity through the Surface Termination of Perovskite Catalysts. *Angewandte Chemie International Edition* **2017,** *56* (33), 9820-9824.
41. Bai, L.; Polo-Garzon, F.; Bao, Z.; Luo, S.; Moskowitz, B. M.; Tian, H.; Wu, Z., Impact of Surface Composition of SrTiO3 Catalysts for Oxidative Coupling of Methane. *ChemCatChem* **2019,** *11* (8), 2107-2117.
42. Rotko, M.; Machocki, A.; Stasinska, B., Studies of catalytic process of complete oxidation of methane by SSITKA method. *Applied Surface Science* **2010,** *256* (17), 5585-5589.
43. Rotko, M.; Zawadzki, W.; Redko, V., Steady state isotopic transient kinetic analysis of the combustion of CH4 over Co-Mn-O catalysts. *Catalysis Communications* **2019,** *125*, 32-36.
44. Royer, S.; Bérubé, F.; Kaliaguine, S., Effect of the synthesis conditions on the redox and catalytic properties in oxidation reactions of LaCo1−xFexO3. *Applied Catalysis A: General* **2005,** *282* (1), 273-284.

TABLE OF CONTENTS